TOWARD POLARIMETRY WITH GREGOR – TESTING THE GREGOR POLARIMETRIC UNIT

A. HOFMANN, J. RENDTEL, and K. ARLT

Astrophysikalisches Institut Potsdam, Sonnenobservatorium Einsteinturm,
An der Sternwarte 16, 14482 Potsdam, Germany

Abstract. The new 1.5 m solar telescope GREGOR with modern scientific instrumentation will become operational in the near future. The GREGOR Polarimetric Unit (GPU) for the calibration of polarimetric measurements with any post-focal device has been developed at the Astrophysical Institute Potsdam (AIP). Here we describe details of the extensive test measurements made in the laboratory of the Solar Observatory "Einsteinturm".

Key words: Sun - instrumentation - high resolution spectro-polarimetry

1. Introduction

GREGOR is a common project of a modern 1.5 m solar telescope (Volkmer et al., 2007) conducted by a German consortium consisting of the Kiepenheuer-Institut für Sonnenphysik in Freiburg (KIS), the Astrophysikalisches Institut Potsdam (AIP), the Institut für Astrophysik in Göttingen (IAG; leaving in 2008), and the Max Planck Institute for Solar System Research (MPS; joining in 2008). Further international partners are the Astronomical Institute Ondřejov (Czech Republic) and the Instituto de Astrofísica de Canarias (Tenerife, Spain). The telescope will become operational in the near future. GREGOR's telescope concept and optical scheme are designed for high spatial resolution as well as high resolution spectro-polarimetry. Among the first post-focus instruments are the GREGOR Fabry Perot Interferometer (GFPI – Puschmann et al., 2006) which is now completed and operated by the AIP (Balthasar et al., 2009) and the Tenerife Infrared Polarimeter II (TIP II – Collados et al., 2007). Both instruments require careful polarimetric calibration which is provided by the GREGOR Polarimetric Unit (GPU), designed and built by the AIP. A

Figure 1: Left: The mechanical structure of the telescope at the top of the building at Izaña/Tenerife. Right: Basic optical scheme of GREGOR. M or F indicate mirrors or foci, respectively. Courtesy of GREGOR-consortium.

general overview is given by Hofmann (2008). Here we describe results of extensive test measurement series carried out in the optical laboratory of the Solar Observatory "Einsteinturm".

2.   The GPU – General remarks

The main function of the GPU is to calibrate any post-focus polarimeter. For this reason it has to fulfill two tasks: (i) it takes care of the instrumental polarization induced by optical components between the calibration optics and the polarimeter; (ii) it calibrates the performance of the polarimeter. The location of the GPU in the optical system of GREGOR is determined by the required accuracy of polarimetric measurements. This accuracy is strongly influenced by instrumental polarization produced by the reflections on mirrors in front of the analyzing system, i.e., any post-focus polarimeter. The effect increases with the angle of reflection. Therefore, the required optimum position to perform the polarimetric calibration is early in the telescope beam, before the rotational symmetry of the light path is broken by any oblique reflection. In this part of the telescope it can be regarded as polarization free at a 10^{-4} level (Sanchez Almeida and Martinez Pillet,
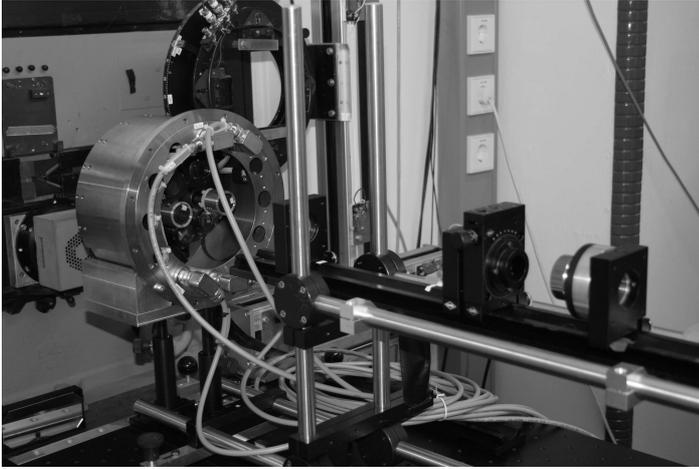
Figure 2: The GPU in front of the spectrograph slit in the laboratory of the Solar Observatory Einsteinturm.

1992). For this reason, the polarimetric unit shall be located in the shadow of the Nasmyth mirror M4 using the narrow beam close to the secondary focus F2 (cf. Figure 1). For further test and adjustment purposes, the GPU provides additional functions. In the non-polarimetric mode, a free aperture and a pinhole are available. The latter allows, for example, the adjustment of the Adaptive Optics system. In the polarimetric mode, components of the calibration optics can be placed in the beam and can be rotated according to the requirements of the calibration scheme. In both modes, a grid target for scale determination and alignment is available.

These functions are implemented by devices mounted on two wheels (see also Figure 2 in Hofmann, 2008) which carry all the needed optical components in precision mounts. An independent and remote control of all functions is provided using a LabView user interface. The mechanical, optical and controlling components have been tested to guarantee the necessary quality.

The calibration optics consists of a linear polarizer (rotatable) and two achromatic quarter wave plates (rotatable) which are in use alternatively for visual range or infrared observations. However, the power density of about 25 W/cm^2 and the large cone angle of the beam ($\pm 5.8°$) are extreme conditions for polarimetry which require new ways for the calibration
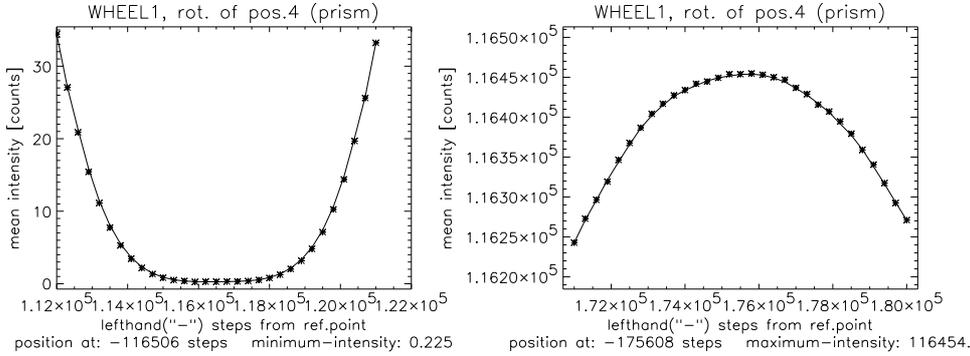
Figure 3: Intensities for rotating the prism in linear polarized light. Left: Rotation around minimum transmission, right: Rotation around maximum transmission.

optics. An air spaced Marple-Hess prism (specific configuration of a double Glan prism) was designed as linear polarizer to withstand the power density and to realize the high distinction ratio of at least 10^{-5} needed. Combined zero-order waveplates of polymethylmetacrylat (PMMA) were designed by Astropribor (Kiev, Ukraine) as superachromatic retarders for the high angular acceptance being necessary.

3.   Testing the Calibration Optics

3.1.   The Linear Polarizer (Prism)

Two linear polarizers adjusted for maximum transition were mounted behind or in front of the GPU, respectively. Thus the prism can be rotated in linear polarized light and the measured intensity depends not from any linear polarization of the light source or the sensitivity of the spectrograph against any linear polarization. The variation of the intensity depends only on the rotation angle φ. With $S2 = \sin 2\varphi$ and $C2 = \cos 2\varphi$, the intensity variation is given by $I' = 0.25 \cdot [(k_1 + k_2) + 2(k_1 - k_2)C2 + (k_1 + k_2)C2^2 + 2k_1 k_2 S2^2]I_o$. There are two maxima and two minima of intensity when rotating the prism by 360°. Two of them are shown in Figure 3 and can be used to obtain the parameters k_1 and k_2 of maximum and minimum transmission. With $k_1 = 116454$ and $k_2 = 0.225$ we achieve an extinction ratio of $er = k_2/k_1 \approx 2 \times 10^{-6}$ or a contrast ratio of $cr = k_1/k_2 \approx 500000 : 1$.
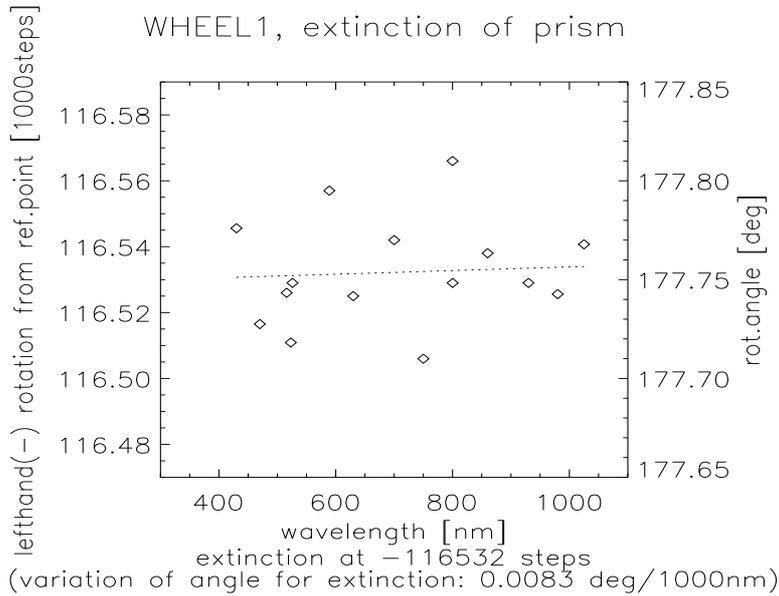
Figure 4: Wavelength dependency for the position of extinction.

The position of the extinction was determined analogously to the left of Figure 3 over a broad range of wavelengths. The measured variation of 0.0083 deg/1000nm lies in the range of errors as shown in Figure 4.

3.2. The Retarders (PMMA Waveplates)

For combined zero-order retarders, the position of the fast axis changes with wavelength. This was measured by the standard method for cirdular retarders, i.e., rotating the retarder between parallel polarizers. The observed intensity is described by $I' = 0.5 \cdot [1 - 1/2 \cdot \sin^2 2\varphi \cdot (1 - \cos \delta)] \cdot I_o$ (φ – rotation angle, δ – retardance). The intensity curve shows maxima when the fast or slow axis are parallel ($\varphi = n \cdot \pi/2$) to the transmission axes of the polarizers and minima when they are 45° between. The procedure is symmetrical by 180°, and, in principle, a rotation over a 180° range is sufficient. We rotated the retarders by a full circle (i.e., 72 intensity measurements per wavelength point) to compensate for residual effects of beam tumbling and to double the number of values included in the calculation of the position angle and retardance. We find four maxima and four minima.
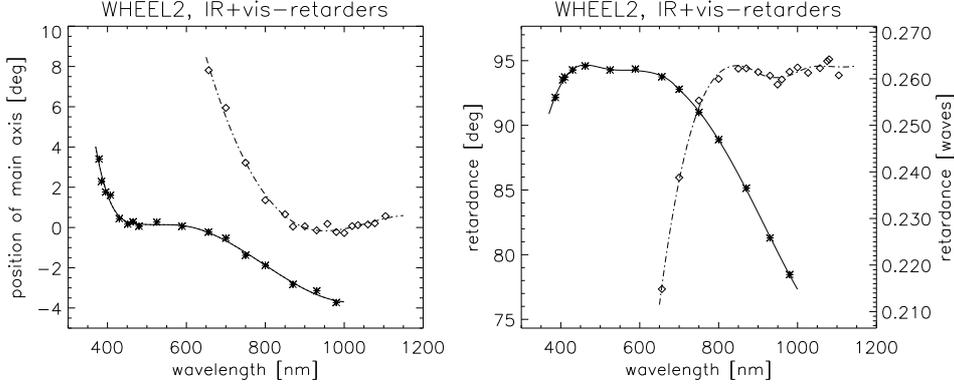
Figure 5: Wavelength dependency for parameters of the retarders for visible (solid lines) and IR (dash-dot lines) spectral range. Left: Position of fast axis, right: Retardance.

The positions and intensities of all extrema were determined by parabolic fits. Measurements were performed in the ranges $379\,\text{nm} - 980\,\text{nm}$ (retarder for visible range) and $656\,\text{nm} - 1105\,\text{nm}$ (retarder for IR-range), respectively. The variation of the position angle is shown in the left part of Figure 5. The ratio between the average of the minima and the average of the maxima is given by $\langle I'_{\min}\rangle / \langle I'_{\max}\rangle = 0.5 \cdot (1 + \cos\delta)$ which can be used to determine the retardances shown in the right part of Figure 5.

4. Calculation of Polarimetric Efficiency

The polarization of the beam leaving the GPU is described by its Stokes-vector which is given by:

$$\vec{S}' = (I', Q', U', V') = \mathbf{G}(\varphi_2, \delta)\, \mathbf{P}(\varphi_1, k_1, k_2) \cdot \vec{S} \tag{1}$$

where $\vec{S}$ is the Stokes-vector of the input beam. $\mathbf{P}$ and $\mathbf{G}$ are the Müller-matrices of the polarizer and the retarder, depending on their rotations φ_1 and φ_2 against any reference system and their transmission parameters k_1 and k_2 or retardation δ, respectively. With $k^+ = k_1 + k_2$, $k^- = k_1 - k_2$, $k^* = k_1 \cdot k_2$, $S_1 = \sin 2\varphi_1$, $C_1 = \cos 2\varphi_1$, $S_2 = \sin 2\varphi_2$, and $C_2 = \cos 2\varphi_2$ we obtain:

$$I' = 0.5 \ (k^+ I + C_1 k^- Q + S_1 k^- U) \tag{2}$$

$$Q' = 0.5 \ (f_{iq} \ I + f_{qq} \ Q + f_{uq} \ U + f_{vq} \ V) \tag{3}$$

where $f_{iq} = [(C_2^2 + S_2^2 \cos \delta)C_1 + S_2 C_2 (1 - \cos \delta) S_1] \ k^-$

$\quad f_{qq} = (C_2^2 + S_2^2 \cos \delta) \ (k^+ C_1^2 + 2k^* S_1^2) + S_2 C_2 (1 - \cos \delta) \ S_1 C_1 (k^+ - 2k^*)$

$\quad f_{uq} = (C_2^2 + S_2^2 \cos \delta) \ S_1 C_1 \ (k^+ - 2k^*) + S_2 C_2 (1 - \cos \delta) \ (k^+ S_1^2 + 2k^* C_1^2)$

$\quad f_{vq} = -2k^* \ S_2 \sin \delta$

$$U' = 0.5 \ (f_{iu} \ I + f_{qu} \ Q + f_{uu} \ U + f_{vu} \ V) \tag{4}$$

where $f_{iu} = [(S_2 C_2 (1 - \cos \delta) \ C_1 + (S_2^2 + C_2^2 \cos \delta) \ S_1] \ k^-$

$\quad f_{qu} = (S_2 C_2 (1 - \cos \delta)(k^+ C_1^2 + 2k^* S_1^2) + (S_2^2 + C_2^2 \cos \delta) S_1 C_1 \ (k^+ - 2k^*)$

$\quad f_{uu} = (S_2 C_2 (1 - \cos \delta) \ (S_1 C_1 (k^+ - 2k^*) + (S_2^2 C_2^2 \cos \delta) \ (k^+ S_1^2 + 2k^* C_1^2)$

$\quad f_{vu} = 2k^* \ C_2 \sin \delta$

$$V' = 0.5 \ (f_{iv} \ I + f_{qv} \ Q + f_{uv} \ U + f_{vv} \ V) \tag{5}$$

where $f_{iv} = [S_2 C_1 - C_2 S_1] \ k^- \sin \delta$

$\quad f_{qv} = [S_2 (k^+ \ C_1^2 + 2k^* \ S_1^2) - (C_2 S_1 C_1 \ (k^+ - 2k^*)] \sin \delta$

$\quad f_{uv} = [S_2 S_1 C_1 (k^+ - 2k^*) - (C_2 (k^+ \ S_1^2 + 2k^* \ C_1^2)] \sin \delta$

$\quad f_{vv} = 2k^* \ \cos \delta$

We select the reference system so that it is related to the transmission axis of the polarizer. In this case, we have $\varphi_1 = 0 \rightarrow C_1 \equiv 1, S_1 \equiv 0$ and the equations are reduced to:

$$I' = 0.5 \ \{(k^+ \ I + k^- \ Q\} \tag{6}$$

$$Q' = 0.5 \ \{(C_2^2 + S_2^2 \cos \delta) \ (k^- \ I + k^+ \ Q)$$
$$\qquad + 2k^* \ [S_2 C_2 (1 - \cos \delta) \ U - S_2 \sin \delta \ V]\} \tag{7}$$

$$U' = 0.5 \ \{S_2 C_2 (1 - \cos \delta) \ (k^- \ I + k^+ \ Q)$$
$$\qquad + 2k^* \ [(S_2^2 + C_2^2 \cos \delta) \ U + C_2 \sin \delta \ V]\} \tag{8}$$

$$V' = 0.5 \ \{S_2 \sin \delta (k^- \ I + k^+ \ Q) - 2k^* \ [C_2 \sin \delta \ U + \cos \delta \ V]\} \tag{9}$$
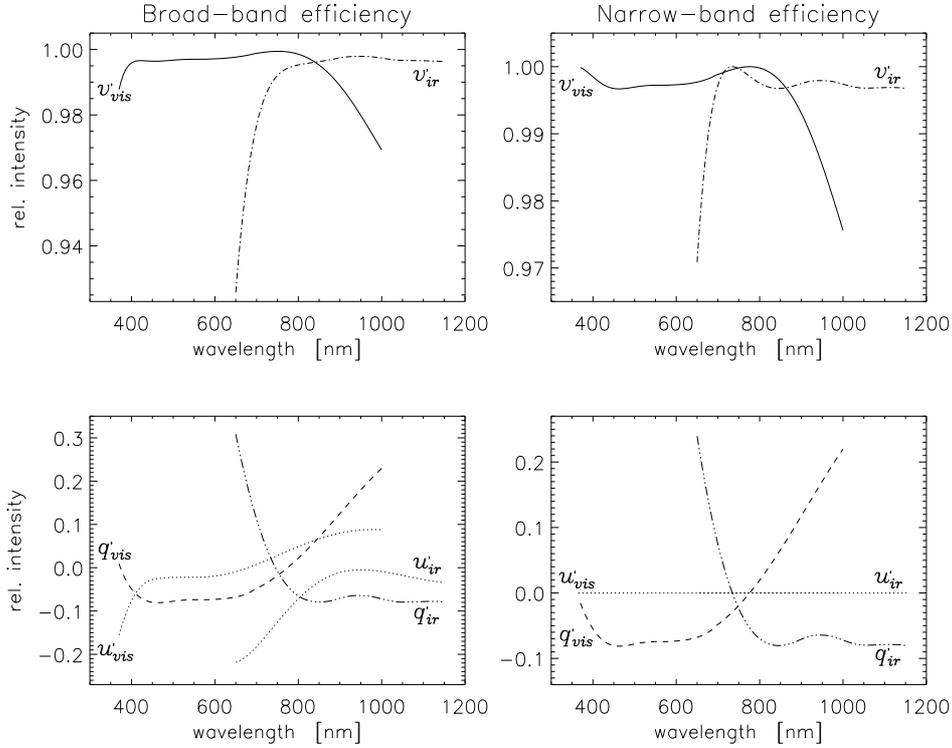
Figure 6: Efficiency of the GPU in generating circular polarized light.

Equations 6–9 can be used to calculate how efficient the polarization optics produces any state of polarization. Figure 6 shows the results if the GPU is in use for generating circular polarization (Stokes-V). The parameters are related to the intensity (I'). In the left-hand graphs is assumed that the retarder is rotated by 45° to the maximum transmission of the prism but fixed to one optimum angle over the whole wavelength range. The right-hand graphs correspond to the typical situation in solar physics where the polarimetry is done in a very narrow spectral range, i.e., in this case the retarder is rotated to the 45°-position of its axis at each wavelength according to the angular behavior shown in the left part of Figure 5. The parameters are found to be very close to the ideal ones $(V' \equiv 1, Q' = U' = 0)$ over the whole wavelength range. These ideal parameters are reached only at the wavelengths where $\delta = 90°$ (exact quarter-wave retardation).

Discussion and Summary

The optical characteristics of the linear polarizers and retarders have been tested in great detail. The parameters are very close to the expected values. But even in the case of deviations from the ideal case, our precise measurements of the parameters will allow to determine the necessary correction matrices. Then, the routines applied to the observational data will allow high precision polarimetric measurements. Of course, it is promising that the necessary corrections are expected to be very small.

The high extinction ratio between 10^{-5} and 10^{-6} of the linear polarizer, the retardation accuracy of $\lambda/100$ of the waveplates, and an accuracy of $0.1°$ for the rotational position angles will enable to measure the Müller-matrices at a 10^{-4} level being a precondition for high-precision measurements of magnetic fields and plasma motions in the solar photosphere and chromosphere down to the aspired scales of $70\,\mathrm{km}$ on the Sun.

References

Balthasar, H., Bello Gonzaález, N., Collados, M., Denker, C., Hofmann, A., Kneer, F., Puschmann, K.: 2009, in *Cosmic Magnetic Fields: From Planets to Stars and Galaxies*, K.G. Strassmeier, A.G. Kosovichev and J. Beckmann, eds. *Proc. IAU Symp. 259*, submitted

Collados, M., Lagg, A., Díaz García, J. J., Hernándes Suárez, E. López López, R., Páez Mañá, E., and Solanki, S. K.: 2007, in *The Physics of Chromospheric Plasmas*, Petr Heinzel, Ivan Dorotovič and Robert J. Rutten, eds. *Proc. of Coimbra Solar Physics Meeting*, *ASP Conf. Ser.* **368**, 611

Hofmann, A.: 2008, *Cent. Eur. Astrophys. Bull.* **232**(1), 17

Martinez Pillet, V. and Sánchez Almeida, J.: 1992, *Astron. Astrophys.* **260**, 543

Puschmann, K.G., Kneer, F., Nicklas, H., and Wittmann, A.D.: 2007, in F. Kneer, K. G. Puschmann, A. D. Wittmann (eds.) Proc.: Modern Solar Facilities - Advanced Solar Science, Universitätsverlag Göttingen, 45

Soltau, D., Berkefeld, T., Volkmer, R.: 2006, in L. M. Stepp (ed.) Proc. SPIE **6267**: Ground-based and Airborne Telescopes, 34

Volkmer, R., von der Lühe, O., Kneer, F., Staude, J., Balthasar, H., Berkefeld, T., Caligari, P., Collados, M., Halbgewachs, C., Heidecke, F., Hofmann, A., Klvana, M., Sobotka, M., Nicklas, H., Popow, E., Puschmann, K., Schmidt, W., Soltau, D., Strassmeier, K., and Wittmann, A.: 2007, in F. Kneer, K. G. Puschmann, A. D. Wittmann (eds.) Proc.: Modern Solar Facilities – Advanced Solar Science, Universitätsverlag Göttingen, p. 39

Cent. Eur. Astrophys. Bull. **vol** (2008) 1, 9

9